FLAME SYNTHESIS OF SINGLE- AND MULTI-WALLED CARBON NANOTUBES AND NANOFIBERS

R.L. Vander Wal
The National Center for Microgravity Research at NASA Glenn Research Center
and
Thomas M. Ticich
Centenary College of Louisiana

INTRODUCTION

Metal-catalyzed carbon nanotubes are highly sought for a diverse range of applications that include nanoelectronics [1], battery electrode material [2], catalysis [3], hydrogen storage media [4] and reinforcing agents in polymer composites [5]. These latter applications will require vast quantities of nanotubes at competitive prices to be economically feasible. Moreover, reinforcing applications may not require ultra-high purity nanotubes. Indeed, functionalization of nanotubes to facilitate interfacial bonding within composites will naturally introduce defects into the tube walls, lessening their tensile strength [6].

Current methods of aerosol synthesis of carbon nanotubes include laser ablation of composite targets of carbon and catalyst metal within high temperature furnaces [7] and decomposition of a organometallics in hydrocarbons mixtures within a tube furnace [8]. Common to each approach is the generation of particles in the presence of the reactive hydrocarbon species at elevated temperatures. In the laser-ablation approach, the situation is even more dynamic in that particles and nanotubes are borne during the transient cooling phase of the laser-induced plasma for which the temperature far exceeds that of the surrounding hot gases within the furnace process tube [9]. A shared limitation is that more efficient methods of nanoparticle synthesis are not readily incorporated into these approaches.

In contrast, combustion can quite naturally create nanomaterials such as carbon black [10]. Flame synthesis is well known for its commercial scalability and energy efficiency [11]. However, flames do present a complex chemical environment with steep gradients in temperature and species concentrations [12,13]. Moreover, reaction times are limited within buoyant driven flows to tens of milliseconds [14]. Therein microgravity can greatly lessen temperature and spatial gradients while allowing independent control of flame residence times. In preparation for defining the microgravity experiments, the work presented here focuses on the effect of catalyst particle size and reactant gas in 1g.

EXPERIMENTAL

Catalyst nanoparticles were generated by means of the well known gas evaporation technique. During resistive heating, an inert gas flow of argon was directed across a boat that contained melted iron, thereby entraining evaporated metal. Scatter from a laser beam intersecting the gas flow downstream of the evaporator provided a visual guide of the vaporization rate and thus a means of feedback control. The resulting catalyst aerosol was then directed to the fuel inlet tube of the burner supporting the pyrolysis flame.

The flame was established on a 0.8-cm outer diameter brass fuel tube running through the center of a McKenna burner. Metal nanoparticles and reactant gases were mixed prior to introduction to this fuel tube so as to establish a uniform mixture. Upon emerging from the fuel tube, the aerosol mixture was heated by the surrounding post-flame gases from a rich, premixed flame supported on the sintered metal surface of the McKenna burner. The premixed flame was fueled by 11.0 slpm air and 1.5 slpm C_2H_2. A 15.2-cm long, 2.5-cm outer diameter steel chimney placed 1 cm above the burner served to stabilize the flame.

Material samples from the flame were obtained by thermophoretic sampling 0.5-cm above the chimney. Transmission electron microscopy (TEM) grids were attached to the probe by a sandwich grid holder consisting of a 0.075-mm thick brass shim with a 2 mm diameter hole exposing both sides of a holey TEM grid, as described previously [15]. Probe dwell times within the flow were kept short (250 ms), thus minimizing probe heating. For the dwell times used here, previous measurements have registered a probe temperature elevation of less than 200 C [16].

RESULTS AND DISCUSSION

Single-walled nanotubes (SWNTs) were produced by Fe particles with CO/H_2 gas mixtures in the flame. We observed a strong dependence of the relative yield with total gas flow within the pyrolysis flame and with the relative concentrations of CO and H_2. Figure 1 shows a HRTEM image of a Fe-catalyzed SWNT. As observed with CO/H_2 mixtures within a high temperature furnace, there was a lack of amorphous carbon coverage on the SWNT walls, indicative of an absence of pyrolysis products within the reacting flow.

In contrast to the SWNTs produced with CO/H_2 mixtures, C_2H_2/H_2 mixtures resulted in amorphous carbon nanotubes (more appropriately considered as nanofibers) composed of nongraphitic walls. Figure 2 shows that the nanotube walls contain short, discontinuous, randomly-oriented graphene segments or short stacks of graphitic lamella. The degree of disorder varies among the multi-walled nanotubes (MWNTs) but in no instance did the nanotubes possess the graphitic quality observed when using CO/H_2 mixtures.

Other structures occasionally observed included short MWNTs grouped in clusters embedded within amorphous carbon. Figure 3 shows an outcrop of such a cluster. These graphitic structures always appeared in groups, never individually. This suggests that either a cluster of particles led to their simultaneous formation or that the clustering reflects their coalescence within the gas flow. Lower carbon concentrations did not significantly decrease the amorphous coating but generally led to disappearance of the clusters altogether. Thus, there appears to be a threshold gas-phase carbon concentration necessary for their growth.

In summary, the following results have been observed; a) SWNTs produced with $CO/H_2/He$ mixtures, b) predominantly nongraphitic MWNTs produced with $C_2H_2/H_2/He$ mixtures, albeit in vastly fewer quantities than the SWNTs produced with CO as carbon containing gas. Given that the flame environments fueled by both CO or C_2H_2 possess similar temperatures and residence times, these factors clearly do not account for the observed differences in reactivity and nanotube structure. Therein a combination of both physical and/or chemical factors likely are responsible. While there is a clear physical size difference between the SWNTs and MWNTs, reflecting that of the catalyst particle, this likely reflects a size dependent chemistry/reactivity.

The very different nanotubes and the strong reactivity difference of the Fe particles towards CO and not C_2H_2 are a manifestation of different nanotube growth mechanisms. To describe SWNT growth by preformed catalyst particles, Dai et al. have proposed a *yarmulke* mechanism whereby a hemispherical cap of carbon forms on the metal catalyst particle [17]. With additional carbon supplied by dissociative adsorption of carbon containing gases, the cap lifts off, forming the closed end of the lengthening nanotube. Growth continues provided favorable temperature and carbon supply are maintained. In this mechanism, the carbon migrates to the growing nanotube by surface diffusion. Thus the particle diameter must closely match those quantized sizes allowed for SWNTs. Notably this mechanism does not account for the formation of nongraphitic MWNTs.

In contrast, the nongraphitic nanotubes reflect a well-established mechanism used to describe carbon filament growth. In this model, carbon containing gases dissociate on the catalyst particle, producing surface carbon. Subsequent carbon atom solvation, diffusion through the particle followed by dissolution (precipitation) from the rear of the particle leads to nanotube (filament) growth [18].

Common to both mechanisms is that the catalyst particle determines the size of the nanotube. A second commonality is that the particle provides the carbon by catalyzing dissociative adsorption of reactant gases. Contrasting the two mechanisms, in the yarmulke mechanism the catalyst particle determines only the nanotube diameter, not its structure which is constrained by energetics to be a single graphitic layer parallel to the growth axis. In the latter mechanism, the catalyst particle not only determines the nanotube diameter but also its morphology. As the carbon is supplied by interstitial lattice sites in the particle, the particle rear facets determine the orientation and pattern of the carbon layers forming the nanotube. Notably in this mechanism, the catalyst particle crystal structure is equated to that of the bulk material.

A critical question to be answered by these mechanisms pertains to the relative reactivities of Fe particles towards the different reactant gases. Similar size particles are exposed to the two reactant gases at similar temperatures. Therein the observed differences likely reflect a size dependent reactivity. The electron density and density of electronic states is a strong function of particle size on the nanometer scale. From bulk single crystal studies, CO and C_2H_2 are known to readily undergo dissociative adsorption upon transition metal surfaces, but by very different mechanisms [19]. After end-on adsorption, dissociation of CO proceeds by donation of electron density from the highest bonding orbital, the 5s M.O. to the metal with concurrent back donation into the 1st antibonding orbital, the 2p M.O. In contrast, C_2H_2 adsorbs parallel to the surface, bridging lattice sites. Direct donation of electron density from the sp orbitals lowers the C-C bond order. Dissociation can occur directly or by insertion of other surface adsorbed species into the weakened C-C bond, thereby "gasifying" one of the carbon atoms. We note that other factors may act independently or synergistically. For example, particle surface restructuring could occur upon CO adsorption as known from bulk single crystal studies [19].

Within this framework, the absence of SWNTs produced by small Fe particles within C_2H_2 mixtures reflects an electronic structure incommensurate with electron density acceptance compared to donation to adsorbed CO. In contrast, the predominance of SWNTs produced by CO and relative lack of MWNTs (some highly graphitic structures were observed) reflects the very high reactivity of small (nanometer or subnanometer) Fe particles towards CO. Their high reactivity selects that portion of the particle size distribution suitable for SWNT formation. With increasing particle size, the electronic structure changes, approaching that of the bulk material. As their properties become more similar to the bulk material, they can catalyze dissociative adsorption in a similar manner as the bulk material. Thus larger Fe particles are able to catalyze C_2H_2 dissociation giving rise to MWNTs.

That larger particles are necessary for nanotube growth in C_2H_2 gas mixtures accounts for their much lower relative yield compared to SWNTs using CO gas mixtures. First, they are not the dominant size class produced by the evaporation source. Secondly, MWNT growth may proceed more slowly than SWNT growth as carbon diffusion through the particle will necessarily possess a higher activation energy than carbon diffusion over a smaller particle surface and likely possess a higher temperature dependence.

ACKNOWLEDGMENTS

REFERENCES

[1]Tans, S.J., Devoret, M.H., Dai, H., Thess, A., Smalley, R.E., Geerligs, L.J., and Dekker, C., Nature 386, 474–477 (1997).

[2] Gao, B. Kleinhammes, A., Tang, X.P., Bower, C., Fleming, L., Wu, Y., and Zhou, O., Chem. Phys. Lett. 307:153–157 (1999).

[3] Rodriquez, N.M., Kim, M.-S., and Baker, R.T.K., J. Phys. Chem., 98:13108–13111 (1994).

[4] Pinkerton, F.E., Wicke, B.G., Olk, C.H., Tibbetts, G.G., Meisner, G.P., Meyer, M.S., and Herbst, J.F., J. Phys. Chem. B104:9460–9467 (2000).

[5] Ajayan, P.M., Stephan, O., Colliex, C. and Trauth, D., Science 265:1212–1214 (1994).

[6] Garg, A., and Sinnott, S.B., Chem. Phys. Lett. 295:273–278 (1998).

[7] Kokai, F., Takahashi, K. Yudasaka, M., Yamada, R., Ichihashi, T. and Iijima, S., J. Phys. Chem. 103:4346–4352 (1999).

[8] Andrews, R., Jacques, D., Rao, A.M., Derbyshire, F., Qian, D., Fan, X., Dickey, E.C. and Chen, J., Chem. Phys. Lett. 303:467–473 (1999).

[9] Arepalli, S., and Scott, C.D., Chem. Phys. Lett. 302;139–145 (1999).

[10] Pratsinis, S.E., AIChE Symp. Ser., Vol. 85 (#270), 1980, 57–68

[11] Ulrich, G.D.,Combust. Sci. and Technol. 4:45–57 (1971).

[12] Santoro, R.J., Yeh, T.T., Horvath, J.J. and Semerjian, H.G., Combust. Sci. and Technol. 53:89–115 (1987).

[13] Smyth, K.C., Miller, J.H., Dorfman, R.C., Mallard, W.G., and Santoro, R.J., Comb. and Flame 62:157–181 (1985).

[14] Roper, F.G., Comb. and Flame 29:219–226 (1977).

[15] Vander Wal, R.L., Choi, M.Y. and Lee, K.-O., Comb. and Flame 102:200–204 (1995).

[16] Vander Wal, R.L., Householder, P.A. and Wright, T.W. III, Appl. Spectrosc. 53:1251–1257 (1999).

[17] Dai, H., Rinzler, A.G., Nikolaev, P., Thess, A., Colbert, D.T. and Smalley, R.E., Chem. Phys. Lett. 260:471–474 (1996).

[18] Rodriguez, N.M., Chambers, A. and Baker, R.T.K., Langmuir 11:3862–3866 (1995).

[19] The Chemical Physics of Solid Surfaces and Heterogeneous Catalysis, (D.A. King and D.P. Woodruff eds.) Elsevier 1990 Part A.
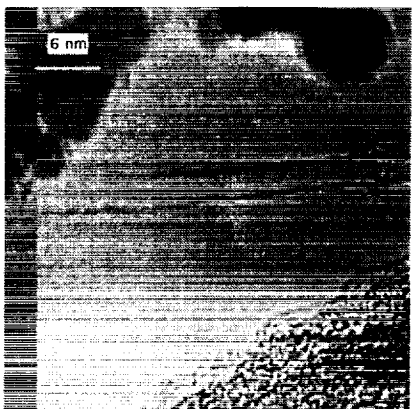
Fig. 1 A HRTEM image of a Fe-catalyzed SWNT produced within the pyrolysis flame with a CO/H$_2$/Ar mixture. The flow rates were 0.5, 0.5 and 0.5 slm respectively.
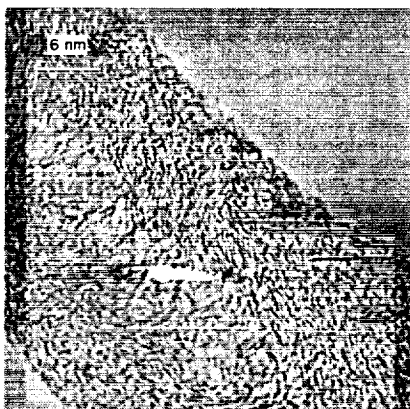
Fig. 2 A HRTEM image of a non-graphitic Fe-catalyzed MWNT produced within the pyrolysis flame using a C$_2$H$_2$/H$_2$/Ar mixture. The flow rates were 0.25, 0.25 and 0.5 slm respectively.
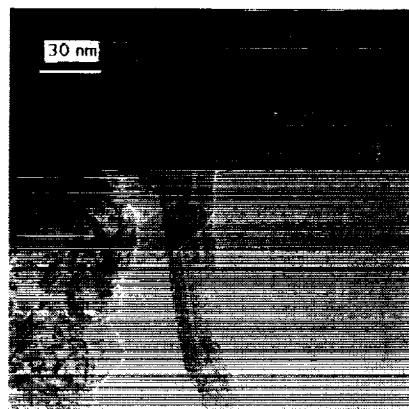
Fig. 3 A HRTEM image of graphitic MWNTclusters, catalyzed by Fe, produced within the pyrolysis flame using C$_2$H$_2$/H$_2$/Ar mixtures.